J Therm Anal Calorim (2012) 110:749–754
DOI 10.1007/s10973-011-1962-2

Thermal and morphological study of Al_2O_3 nanofibers derived from boehmite precursor

Lingli Peng · Xiangyu Xu · Zhi Lv · Jiaqing Song · Mingyuan He · Qian Wang · Lijun Yan · Yang Li · Zhaofei Li

Received: 13 September 2011 / Accepted: 26 September 2011 / Published online: 13 October 2011

Abstract The boehmite nanofibers were prepared by using $NaAlO_2$ and $Al_2(SO_4)_3$ as the starting materials without any surfactant. The phase transitions of the boehmite nanofibres against different temperature were studied and various phases were derived from well-crystallized boehmite nanofibers. All these phases had the same morphology even after high temperature calcination. In addition, the retention of specific surface area of the samples were very high because of the limited aggregation occurred in calcinations for each sample. For instance, the γ-Al_2O_3 obtained at 500 °C had the specific surface area (208.56 m^2/g) with an average pore diameter of 6.0 nm. With the further increase of the calcination temperature, the nanofibers became shorter and coarsening, which resulted in the decrease of the specific surface area. It is worthwhile to notice that the BET surface areas (40.97 m^2/g) and the pore volume (0.27 cm^3/g) of the fibrous structures obtained after 1200 °C calcination are substantially higher than that of the non-fibrous alumina because of the morphology maintenance.

Keywords Boehmite · Nanofiber · Al_2O_3 · Calcination

L. Peng · X. Xu · Z. Lv · J. Song (✉)
State Key Laboratory of Chemical Resource Engineering, Beijing University of Chemical Technology, Beijing 100029, China
e-mail: songjq@mail.buct.edu.cn

M. He
Shanghai Key Laboratory of Green Chemistry and Chemical Processes, East China Normal University, Shanghai 100029, China

Q. Wang · L. Yan · Y. Li · Z. Li
Petrochemical Research Institute of Petrochina, Beijing 100195, China

Introduction

Alumina (Al_2O_3), besides its stable phase α-Al_2O_3, has a variety of metastable structures, including γ-, η-, θ-, and δ-Al_2O_3 [1, 2].. Those Al_2O_3 are widely used as sorbent [3] or support for catalysts [4, 5] in refining [6–12], petrochemicals and fine chemicals processes [13]. The usefulness of a specific alumina in each of these processes requires a favorable combination of textural properties, including surface area, pore volume, and pore size distribution as well as the surface acid/base characteristics. To this end, considerable efforts have been directed toward the preparation of nanostructure Al_2O_3. Various morphologies of Al_2O_3, such as membrane [14], nanowires [15], nanosheets [16], nanobelts [15], nanofibers [17, 18], and whiskers [19] had been obtained by a variety of methods in the past a few years. The concept of surfactant templating has been introduced into the synthesis of most nanostructured Al_2O_3, which cause high cost and environmental problems. Hence, a template free approach to the preparation of nanostructured Al_2O_3 would be highly appreciated.

Normally, conventional Al_2O_3 formed through the thermal dehydration of a crystalline boehmite via a sequential metastable transition: Boehmite $\rightarrow \gamma \rightarrow \delta \rightarrow \theta \rightarrow \alpha$-$Al_2O_3$ [20–22]. However, most Al_2O_3 derived from solution precursors often have atomically disordered framework walls that lack the structural stability and surface characteristics of a transition alumina. As a result, γ-Al_2O_3 can be obtained at temperatures above 800 °C [23, 24], but such conditions inevitably compromise the poor structure and cause a drastic deterioration in textural properties because of the sintering of the primary particles and consequential framework contraction [23–25]. More severely deteriorated are δ-, θ-, α-Al_2O_3 formed at even higher temperatures. So far, the preparation of high surface

area alumina samples formed at high temperatures is still demanding and challenging.

In this study, we prepared the boehmite nanofibers in the absence of any surfactant [26–28], and studied their phase transitions and morphology changes.

Experimental

Preparation of the boehmite nanofibers

The boehmite nanofibers were synthesized as follows: 100 mL of $NaAlO_2$ solution containing 29.5 g $NaAlO_2$ (0.36 mol)was added dropwise to 0.4 mol/L $Al_2(SO_4)_3$ solution with vigorous stirring, and the stirring were kept until a homogeneous solution was formed. The obtained suspension (pH ~8.5) was sealed into a Teflon-lined stainless autoclave and kept at 180 °C for 24 h without any stirring or shaking. A white precipitate was recovered. The precipitate was then centrifuged, washed, and dried in air at 60° for 24 h to obtain the boehmite nanofibers.

Preparation of the Al_2O_3 nanofibers

The boehmite nanofibers were calcined at 400, 450, 500, 600, 700, 800, 1000, and 1200 °C for 2 h to convert the boehmite to Al_2O_3. The temperature ramp rate was 10 °C/min.

Analysis and characterization

X-ray powder diffraction (XRD) patterns were recorded on a Rigaku D/MAX 2500 X-ray diffractometer with a graphite monochromator and Cu Kα radiation ($\lambda = 1.54178$ Å). Thermogravimetry and differential thermal analysis (TG-DTA) curves were obtained on a Q600SDT TGA-DTA-DSC Synchronous detector in the temperature range 10–1000 °C with a heating rate at 10 °C/min^{-1} in N_2 flow (100 mL/min). The specific surface area, pore volume, and pore size were measured using the N_2 sorption method with a Micromeritics ASAP 202 instrument. A GEOL-2100 microscope transmission emission microscopy (TEM) was used to identify the crystal structure of the samples.

Results and discussion

The powder XRD patterns of the boehmite nanofibers and various Al_2O_3 samples obtained at 400, 450, 500, 600, 700, 800, 1000, and 1200 °C are shown in Fig. 1. The XRD pattern of the boehmite nanofibers (Fig. 1a) exhibit the typical reflections of boehmite phase (Ref: JCPDS no. 21-1307) without any impurity peak. The strong sharp reflections indicate that the boehmite nanofibers have a well-formed crystalline structure. It can be seen that diffraction peaks of the sample obtained at 400 °C (Fig. 1b) were the same as that of boehmite, which indicates that the boehmite nanofibers are stable at 400 °C. Fig. 1c exhibits the typical reflections of γ-Al_2O_3 phase (Ref: JCPDS no. 10-0425), which proves that the boehmite structure transformed to γ-Al_2O_3 when the calcinations temperatures were between 400 and 450 °C. The γ-Al_2O_3 structure was well maintained until the calcination temperature up to 800 °C, as shown in Fig. 1d–g. When the calcination temperature was raised to 1000 °C, new diffraction peaks emerged at 32.8, 45.6, 46.5, and 66.9°, respectively, which should be attributed to δ-Al_2O_3, as shown in Fig. 1h. With a further increase of the calcination temperature from 1000 to 1200 °C, the samples transited to hybrid phases with θ-Al_2O_3 (Ref: JCPDS no. 35-0121) and α-Al_2O_3 (Ref: JCPDS no. 10-173).

The mass loss of the boehmite nanofibers was measured by TG-DTA method to investigate the thermal behavior and mass change during the calcination process [29, 30]. The measured TG-DTA-DTG curves of the boehmite nanofibers are shown in Fig. 2. It exhibits four mass loss steps according to the TG curve and two endothermic peaks in the DTA curve. The endotherm peak centered at 78.9 °C and mass loss to ~224.6 °C corresponds to the removal of surface adsorbed water with the associated mass loss of 3.7%. A second mass loss at 224.6–526.6 °C with an endotherm peak centered at 481.1 °C can be attributed to the removal of the hydroxyl group, which corresponds to the lattice changes coinciding with the transformation of boehmite to γ-Al_2O_3 [31]; the associated mass loss was 12.9%. This is in agreement with the XRD results, as shown in Fig. 1. The third step (526.6–800.9 °C) is related to the further dehydroxylation of the γ-Al_2O_3 [32, 33]; the associated mass loss was 1.1%. The last mass loss

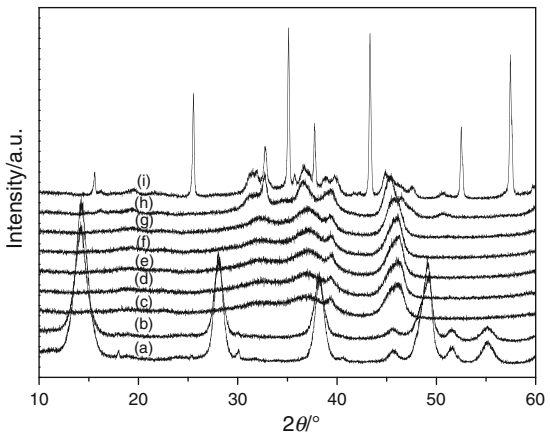

Fig. 1 XRD patterns of the boehmite nanofibers (**a**) and samples obtained at (**b**) 400 °C, (**c**) 450 °C, (**d**) 500 °C, (**e**) 600 °C, (**f**) 700 °C, (**g**) 800 °C, (**h**) 1000 °C, (**i**) 1200 °C

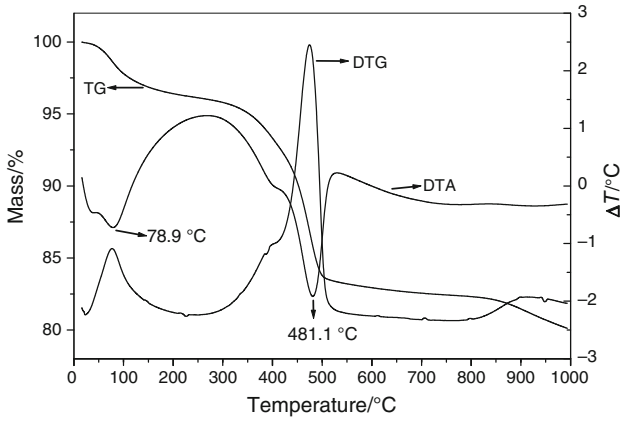

Fig. 2 TG-DTA-DTG curves of the boehmite nanofibers

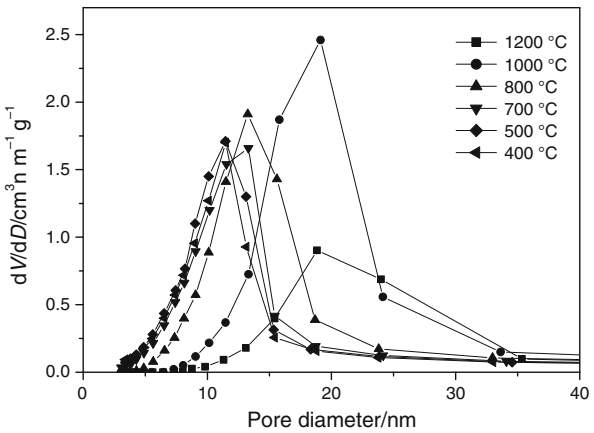

Fig. 4 The pore size distributions of samples obtained at different calcination temperature

between 800.9 and 1000 °C corresponds to the formation of δ-Al_2O_3.

Figure 3 show the TEM images of the boehmite nanofibers and the samples calcined at 400, 450, 500, 700, 800, 1000, and 1200°, respectively. It can be seen that the starting boehmite nanofibers have a length over 50 nm and a thickness of about 6 nm (Fig. 3a). And all the samples obtained at different temperature show similar fibrous morphology, even at 1200°. It implies that the fibrous structure has strong resistance to sintering even if they were calcined at high temperatures. The thickness of nanofibers is 7–8 nm after calcined at 400 °C for 2 h. It becomes finer (6–7 nm) with the increase of calcination temperature from 400 to 500 °C. This is related to the combined effect of dehydration and condensation as above mentioned. Half of the oxygen atoms from the boehmite layers are removed because of condensation of protons and hydroxyls between layers, thus, causing the rearrangement which leads to the phase transitions. The phase transition is accompanied by a decrease in the size of the crystallites. With the increase of the calcination temperature, the

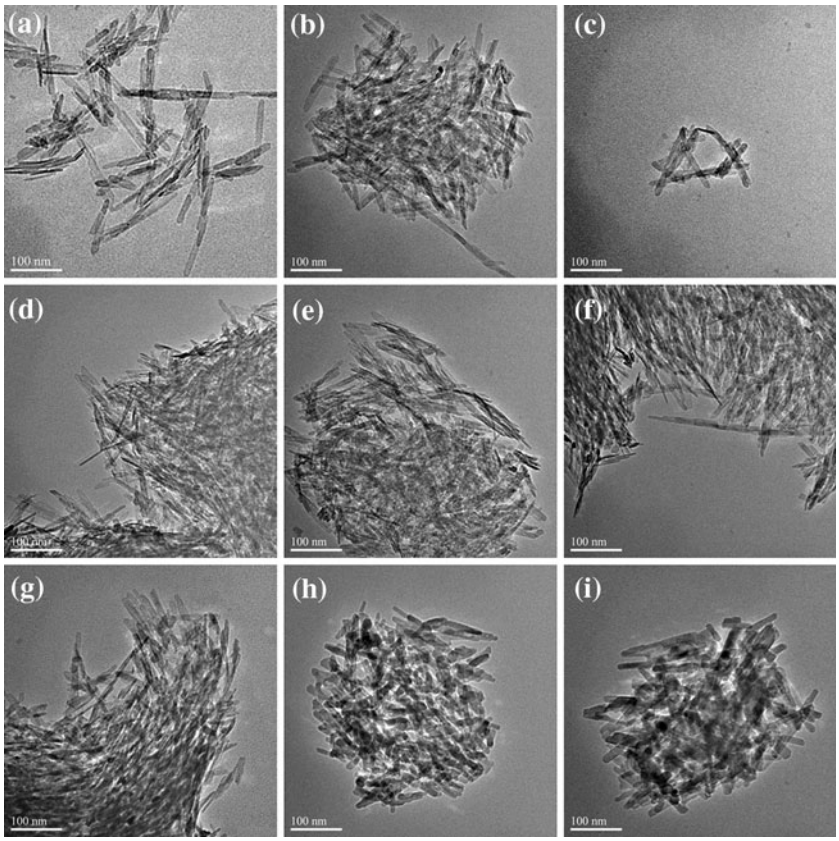

Fig. 3 TEM images of the boehmite nanofibers (**a**) and the samples obtained at (**b**) 400 °C, (**c**) 450 °C, (**d**) 500 °C, (**e**) 600 °C, (**f**) 700 °C, (**g**) 800 °C, (**h**) 1000 °C, (**i**) 1200 °C

Table 1 Properties of the boehmite nanofibers and Al_2O_3 obtained at various temperatures

T/°	S_{BET}/m^2/g^{-1}	Pore volume/cm^3/g	D/nm	Calculated surface areas/m^2/g^{-1}	Phase identification
400	179.59	0.47	7.5	177.18	Boehmite
450	195.65	0.54	6.5	192.31	γ-Al_2O_3
500	208.56	0.53	6.0	208.33	γ-Al_2O_3
600	198.23	0.51	6.2	201.61	γ-Al_2O_3
700	172.81	0.49	7.0	178.51	γ-Al_2O_3
800	144.80	0.54	8.5	147.06	γ-Al_2O_3
1000	92.66	0.54	12.6	93.37	δ-Al_2O_3
1200	40.97	0.27	24.5	41.86	θ-Al_2O_3 + α-Al_2O_3

average diameter of the Al_2O_3 nanofibers is enlarged from 6.0 nm at 500 °C to 24.5 nm at 1200 °C, while the length was reduced simultaneously.

Figure 4 shows the pore size distributions of all the Al_2O_3 samples obtained at different calcination temperature, which were calculated from N_2 isotherms measurements by using the Barrett-Joyner-Halenda method [34]. The calculated results of all the samples are listed in Table 1. The pore volume should be attributed to the inter-crystallite voids of the randomly stacked alumina nanofibers. The broad distributions of pore size of the samples are owing to the random stacking and irregular shape of the voids. The most probable pore size is about 11 nm in a range of 3–40 nm for γ-Al_2O_3 obtained at 500°. It can be seen that both the most probable pore size and the width of the pore distribution at half height are increasing with the increase of calcination temperature. However, the pore volume is almost constant for the samples calcined between 400 and 1000 °C. It confirms the pore volume contribution to the inter-crystallite voids of the randomly stacked alumina nanofibers. When the calcination temperature rise from 1000 to 1200 °C, the samples convert to hybrid phases of θ-Al_2O_3 and α-Al_2O_3, the fibrous structure appear faint sintering accompanying the decrease of pore volume. However, the samples always retained the property of being porous, which induced by the fibrous structure that has considerable strong resistance to sintering during calcination.

The specific surface areas calculated from fibrous size observed from TEM measurements are consistent with the experimental values as shown in Table 1, which suggests the samples are monodispersed nanoparticles. This is in good agreement with the TEM images (Fig. 3) and explains the almost invariable pore volume between 400 and 1000 °C. The γ-Al_2O_3 nanofibers obtained at 500° has the highest specific surface area with average pore diameter of 6.0 nm according to Table 1. There is an increase of specific surface area with the increase of calcination temperature from 400 to 500 °C. It is related to the finer fibers brought by the combined effect of dehydration and condensation. The phase conversion is followed by a decrease in the size of the crystallites and a corresponding increase in the specific surface area. It can be seen that there is a descending trend for the specific surface area as the calcination temperature increased from 500 to 1200 °C. The first event in the temperature range 500–800 °C is attributed to the coarsening and shortening of γ-Al_2O_3 nanofibers. The second event from 800 to 1200 °C is because of the transition of γ- to α-Al_2O_3 and the coarsening of Al_2O_3 nanofibers. The transition of γ- to α-Al_2O_3 involves a reconstructive recrystallization process, which leads to the fibrous structure faint sintering. In this article, the fibrous δ-Al_2O_3 appears when the calcination temperature increased to 1000° accompanying the almost invariable pore volume. The result of the specific surface areas calculated from TEM images in agreement with S_{BET} obtained from BET measurement suggests that δ-Al_2O_3 is monodispersed nanosize particles. It is reasonable to deduce that the main fall of the specific surface area is related to the coarsening and shorten of Al_2O_3 nanofibers. After calcined at 1200 °C for 2 h, the specific surface area is 40.97 m^2/g^{-1}, and the remaining pore volume was 0.27 cm^3/g. Even though, it is still substantially larger in comparison with the non-fibrous Al_2O_3 because of the maintenance of fibrous shape [23, 35–37]. As a result, such a fibrous structure exhibits large porosity and strong resistance to sintering when calcined at high temperatures so that these Al_2O_3 nanofibers can be used as supports for catalysts working at high temperatures, for instance, such as combustion catalysts.

Conclusions

In this study, the variations in the structure of fibrous crystallites of alumina, derived by calcinations of the well-crystallized boehmite nanofibers at different temperatures in air were investigated. The morphology retention of the prepared nanofibers during the transformation from boehmite to α-Al_2O_3 is exceedingly good. With the increase of

calcination temperature, the shape of the Al_2O_3 nanofibers becomes shorter and coarsening, inducing a gradual decrease of the specific surface area. The specific surface area and the pore volume of Al_2O_3 obtained after 1200 °C calcination can attain values of 40.97 m^2/g^{-1} and 0.27 cm^3/g, respectively, which can be attributed to the high retention of its fibrous shape.

Acknowledgements The authors are grateful to the financial support from 863 Program (2009AA064201 and 2010AA03A403).

References

1. Stumpf HC, Russell AS, Newsome JW, Tucker CM. Thermal transformations of aluminas and alumina hydrates. Ind Eng Chem. 1950;42:1398–403.
2. Ruan HD, Frost RL, Kloprogge JT. Comparison of Raman spectra in characterizing gibbsite, bayerite, diaspore, and boehmite. J Raman Spectrosc. 2001;32:745–50.
3. Martínez A, Prieto G, Rollán J. Nanofibrous γ-Al2O3 as support for Co-based Fischer-Tropsch catalysts: pondering the relevance of diffusional and dispersion effects on catalytic performance. J Catal. 2009;263:292–305.
4. Maity SK, Flores L, Ancheyta J, Fukuyama H. Carbon-modified alumina and alumina-carbon-supported hydrotreating catalysts. Ind Eng Chem Res. 2009;48:1190–5.
5. Ryan MR, John RC, Kim WG, John CC, Carsten S. Structural changes of γ-Al_2O_3-supported catalysts in hot liquid water. ACS Catal. 2011;1:552–61.
6. Le Page JF. Applied heterogeneous catalysis-design, manufacture, use of solide catalysts, Paris: Editions Technip; 1987.
7. Raybaud P, Costa D, Valero MC, Arrouvel C, Digne M, Sautet P, Houlhoat H. First principles surface thermodynamics of industrial supported catalysts in working conditions. J Phys: Condens Matter. 2008;20:64–74.
8. Charles M, Eswar A, Melaz TF, Denis U. Asphaltene diffusion and adsorption in modified NiMo alumina catalysts followed by ultraviolet (UV) spectroscopy. Energy Fuels. 2010;24:4290–300.
9. Ying ZS, Gevert B, Otterstedt JE, Sterte J. Hydrodemetallisation of residual oil with catalysts using fibrillar alumina as carrier material. Applied Catalysis A. 1997;153:69–82.
10. Kurikka VP, Shafi M, Ulman A, Lai J, Yang NL, Cui MH. A new route to alumoxane gel: a versatile precursor to γ-alumina and alumina-based ceramic oxides. J Am Chem Soc. 2003;125:4010–1.
11. Trombetta M, Busca G, Rossini S, Picolli V, Cornaro U, Guercio A, Catani R, Willey RJ. FT-IR studies on light olefin skeletal isomerization catalysis: III. Surface acidity and activity of amorphous and crystalline catalysts belonging to the SiO_2–Al_2O_3 system. J Catal. 1998;179:581–96.
12. Wildschut J, Mahfud FH, Venderbosch RH, Heeres HJ. Hydrotreatment of fast pyrolysis oil using heterogeneous noble-metal catalysts. Ind Eng Chem Res. 2009;48:10324–34.
13. Hwang J, Min BD, Lee JS. Al_2O_3 nanotubes fabricated by wet etching of ZnO/Al_2O_3 core/shell nanofibers. Adv Mater. 2004;16:422–5.
14. Ozao R, Yoshida H, Inada T. Morphological and structural change of nano-pored alumina membrane above 1200 K. J Therm Anal Calorim. 2002;69:925–31.
15. Wang YW, Zhang LD, Meng GW, Peng XS, Jin YX, Zhang J. Fabrication of ordered ferromagnetic-nonmagnetic alloy nanowire arrays and their magnetic property dependence on annealing temperature. J Phys Chem B. 2002;106:2502–7.
16. Zhao Y, Frost RL, Vágvölgyi V, Waclawik ER, Kristóf J, Horváth E. XRD, TEM and thermal analysis of yttrium doped boehmite nanofibres and nanosheets. J Therm Anal Calorim. 2008;94:219–26.
17. Zhu HY, Riches JD, Barry JC. γ-Alumina nanofibers prepared from aluminum hydrate with poly(ethylene oxide) surfactant. Chem Mater. 2002;14:2086–93.
18. Zhao Y, Frost RL, Martens WN, Zhu HY. XRD, TEM and thermal analysis of Fe doped boehmite nanofibres and nanosheets. J Therm Anal Calorim. 2007;90:755–60.
19. Yu ZQ, Du YW. Preparation of nanometer-sized alumina whiskers. J Mater Res. 1998;13:3017–8.
20. Frost RL, Kloprogge JT, Russell SC, Szetu J. Dehydroxylation of aluminum (oxo)hydroxides using infrared emission spectroscopy. Part II: boehmite. Appl Spectrosc. 1999;53:572–82.
21. Palmero P, Bonelli B, Lomello F, Garrone E, Montanaro L. Role of the dispersion route on the phase transformation of a nanocrystalline transition alumina. J Therm Anal Calorim. 2009;97:223–9.
22. Palmer SJ, Frost RL. Thermal decomposition of Bayer precipitates formed at varying temperatures. J Therm Anal Calorim. 2010;100:27–32.
23. Palmero P, Lombardi M. Sintering of a nano-crystalline metastable alumina Influence of the firing parameters on the phase development and microstructural evolution. J Therm Anal Calorim. 2009;97:191–6.
24. Balek V, ubrt J, Rouquerol J, Llewellyn P, Zeleòák V, Bountsewa IM, Beckman IN, Györyová K. Emanation thermal analysis study of synthetic gibbsite. J Therm Anal Calorim. 2003;71:773–82.
25. Koga N. A comparative study of the effects of decomposition rate control and mechanical grinding on the thermal decomposition of aluminum hydroxide. J Therm Anal Calorim. 2005;81:595–601.
26. Zhao Y, Frost RL, Martens WN, Zhu HY. Growth and surface properties of boehmite nanofibers and nanotubes at low temperatures using a hyrothermal synthesis route. Langmuir. 2007;23:9850–9.
27. Hao LC, Yu WD. Evaluation of thermal protective performance of basalt fiber nonwoven fabrics. J Therm Anal Calorim. 2010;100:551–5.
28. Zhu HY, Gao XP, Song DY, Bai YQ, Ringer SP, Gao Z, Xi YX, Martens WN, Riches JD, Frost RL. Growth of boehmite nanofibers by assembling nanoparticles with surfactant micelles. J Phys Chem B. 2004;108:4245–7.
29. Maclver DS, Tobin HH, Barth RT. Catalytic aluminas I. Surface chemistry of eta and gamma alumina. J Catal. 1963;2:485–97.
30. Maclver DS, Wilmot WH, Bridges JM. Catalytic aluminas: II. Catalytic properties of eta and gamma alumina. J Catal. 1964;3:502–11.
31. Gianluca P, Craig EB, Andrew LR, Robert DH, Kartsen W, Andrew JS, Brett AH, John VH. Boehmite derived γ-alumina system. 1. Structural evolution with temperature, with the identification and structural determination of a new transition phase, γ-alumina. Chem Mater. 2004;16:220–36.
32. Kloprogge JT, Ruan HD, Frost RL. Thermal decomposition of bauxite minerals: infrared emission spectroscopy of gibbsite, boehmite and diaspore. J Mater Sci. 2002;37:1121–9.
33. Gonçalves MLA, Barreto JRC, Cerqueira WV, Teixeira AMRF. Effect of zeolite, kaolin and alumina during cracking of heavy petroleum residue evaluated by thermogravimetry. J Therm Anal Calorim. 2009;97:515–9.

34. Barrett EP, Joyner LG, Halenda PH. The determination of pore volume and area distributions in porous substances: I. Computations from nitrogen isotherms. J Am Chem Soc. 1951;73:373–80.
35. Pierre AC, Elaloui E, Pajonk GM. Comparison of the structure and porous texture of alumina gels synthesized by different methods. Langmuir. 1998;14:66–73.
36. Zhang XX, Ge YL, Hannula SP, Levanen E, Mantyla T. Nanocrystalline a-alumina with novel morphology at 1000 °C. J Mater Chem. 2008;18:2423–5.
37. Zhang XX, Honkanen M, Levanen E, Mantyla T. Transition alumina nanoparticles and nanorods from boehmite nanoflakes. J Cryst Growth. 2008;310:3674–9.